ACS APPLIED MATERIALS & INTERFACES

Research Article

www.acsami.org

Low-Potential Synthesis of "Clean" Au Nanodendrites and Their High Performance toward Ethanol Oxidation

Jiu-Ju Feng,[†,‡] Ao-Qi Li,[†] Zhen Lei,[†] and Ai-Jun Wang*[,†,‡]

[†]Key Laboratory of Green Chemical Media and Reactions, Ministry of Education; School of Chemistry and Environmental Science, Henan Normal University, Xinxiang 453007, China

[‡]College of Chemistry and Life Science, College of Geography and Environmental Science, Zhejiang Normal University, Jinhua 321004, China

Supporting Information

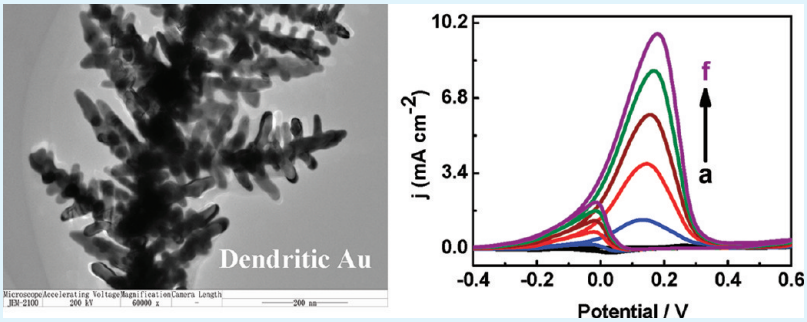

ABSTRACT: The shape control of Au nanocrystals is crucial to their catalytic applications and optical properties. Well-defined Au nanodendrites (NDs) have been prepared on a glassy carbon electrode using low-potential synthesis, assisted by ethylenediamine (EDA). The effects of applied potential, deposition time, and $HAuCl_4$ (or EDA) concentrations on the morphology of the Au deposits are discussed in our work. The growth mechanism can be explained by a two-staged growth of dendrites: initial branching and subsequent dendritic growth. The Au NDs exhibits superior catalytic performance toward ethanol oxidation, in comparison with the polycrystalline Au nanoparticles. The simple and facile synthetic technique can be applied to the construction of other metals with complex hierarchical structures on a large-scale.

KEYWORDS: *electrodeposition, ethylenediamine, Au dendrites, catalysis, ethanol*

INTRODUCTION

Au nanocyrstals have attracted great interests because of their unique physic and chemical properties, which have widespread applications in optics, electronics, sensors, catalysis, surface-enhanced Raman scattering (SERS), and self-cleaning functions.[1−6] Their shape-controlled synthesis and relevant applications have received great success in the past few years for their size and shape dependent properties. Another reason is due to small surface energy difference between different surfaces of Au. The small energy barrier between different morphologies can be easily overcome by fine-adjusting the reaction parameters. Many of Au nanocrystals are usually assembled into different hierarchical structures, which have highly open surfaces and promising for catalytic applications.[7,8] However, surface-dependent catalysis performances of Au nanocrystals were less explored until now.

To date, many efforts have been devoted to the fabrication of Au nanostructures with various morphologies,[9] including flowers,[10] particles,[11] wires,[12] pillars,[13] and dendrites.[14−18] Among them, Au dendrites are particularly popular, since they have long main trunks and parallel secondary branches with sharp edges or tips, as well as nanoscale junctions.[19] The special structures bring potential and practical applications in (bio)sensors, electronics, catalysis, SERS, and fuel cells.[20,21]

In general, a variety of Au dendrites have been prepared by many methods, such as surfactant-directed synthesis,[22,23] galvanic replacement synthesis,[16,24] and electrochemical synthesis with the help of small molecules.[25−27] Qin and co-workers[16] prepared single-crystalline dendritic Au nanostructures in a ionic liquid solution of tetrachloroaurate (1-butyl-3 methylimidazolium hexafluorophosphate). Tang et al.[17] obtained dendritic Au nanoparticles with poly(N-vinyl-2-pyrrolidone) under hydrothermal conditions. Huang and co-workers[23] synthesized Au dendrites using the complexes of dodecyltrimethylammonium bromide and β-cyclodextrin.

Synthesis of metallic nanodendrites by chemical reactions is usually time-consuming, complicated, and extensive use of chemicals.[9,20,28] Alternatively, electrodeposition is a facile, feasible, and cost-effective method, which can make the dendritic structures directly deposited on a electrode sur-

Received: February 10, 2012
Accepted: April 23, 2012
Published: April 23, 2012

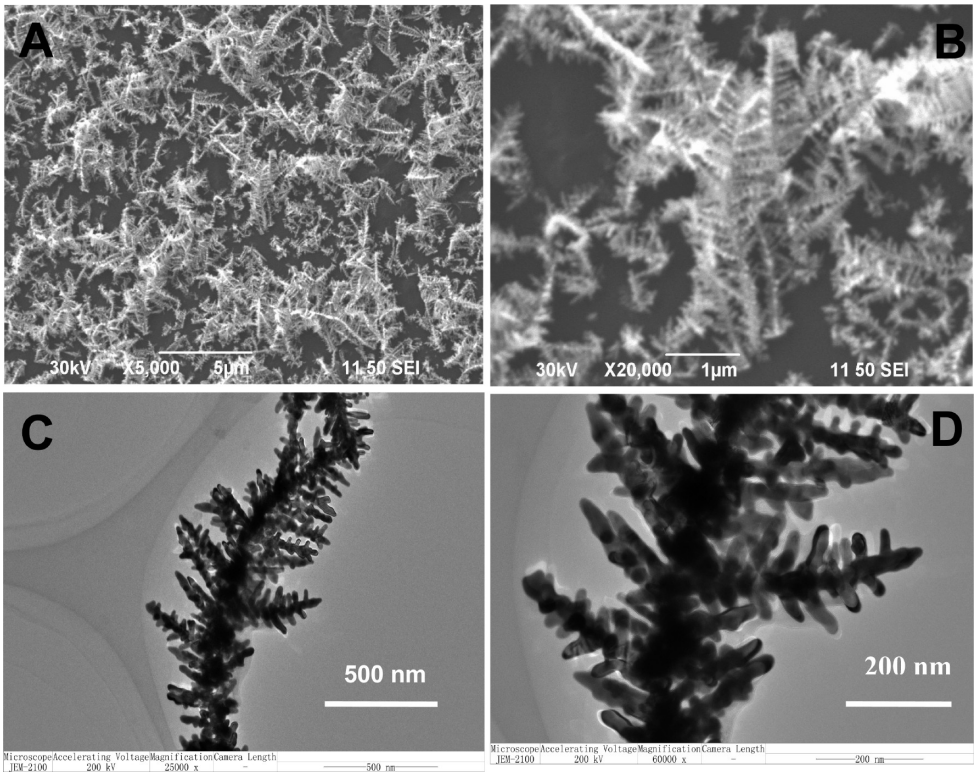

Figure 1. Typical SEM (A, B) and TEM (C, D) images of the Au NDs with different magnification on the GCE under the typical synthesis of 0.0 V (vs SCE) for 600 s in the electrolyte containing 2.5 mM $HAuCl_4$, 0.5 M H_2SO_4, and 150 mM EDA.

face.[27,29] Moreover, the growth rate can be readily and independently controlled by precise-adjusting the interplay between the rate of crystal growth and mass transport. Additionally, the electrodeposits are highly pure and uniform. Up to now, a couple of strategies have been proposed in the synthesis of Au dendritic structures. Ye and co-workers[30] prepared gold microdendrites on indium tin oxide electrodes with the aid of Na_2SO_4. Lately, Huang et al. fabricated Au dendrites on a platinum surface with iodide.[31] Lin and co-workers[29] constructed dendritic Au nanostructures with the help of cysteine.

In this study, we developed a facile and template-free method for electrodeposition of "clean" Au nanodendrites (NDs) with the assistance of ethylenediamine (EDA) for initial branching. The effects of the experimental parameters have been discussed in some detail. Compared to polycrystalline Au nanoparticles, the as-prepared Au NDs possess definitely "clean" surface and larger surface area, allowing it to exhibit better catalytic activity toward ethanol oxidation, which might be a promising candidate for fuel cells applications.

EXPERIMENTAL DETAILS

Materials and Apparatus. Chloroauric acid tetrahydrate ($HAuCl_4{\cdot}4H_2O$), H_2SO_4, NaOH, and anhydrous ethanol (C_2H_5OH) were purchased from Beijing Chemical Works (Beijing, China). Other reagents were analytical grade and used without further purification. All of the aqueous solutions were prepared with twice-distilled water.

The samples were characterized using X-ray diffraction (Bruker-D8-AXS diffractometer system equipped with Cu Kα radiation), field emission scanning electron microscopy (SEM, JEOL JSM-7500F), and energy dispersive X-ray spectroscopy (EDX, (JEOL, JSM-7500F equipped with an X-ray energy dispersive spectrometer, operated at 15 kV).

Moreover, low and high resolution transmission electron microscope (HRTEM) observations, coupled with X-ray energy dispersive spectroscopy (EDS) analysis, were also conducted on a JEM-2010HR transmission electron microscope coupled with an energy-dispersive X-ray spectrometer (Dxford-1NCA) operating at 200 kV. Specifically, a small amount of the as-prepared Au deposits was prepared by ultrasonic dispersion into ethanol for TEM observations. Then, the suspension was dropped onto a conventional Cu grid and dried in air before analysis. The elemental composition of the Au NDs was determined by EDS analyzer equipped with the microscope.

All electrochemical experiments were conducted using a CHI 660D electrochemical workstation (Shanghai Chenhua Instrumental Co., Ltd., China). A conventional three-electrode system was used, employing a platinum wire as the counter electrode, a saturated calomel electrode (SCE) as the reference electrode, and a glassy carbon electrode (GCE, 3 mm in diameter) as the working electrode, respectively. Furthermore, the real area of the working electrode was measured according to previous report.[32] All experiments were performed at room temperature, if not stated otherwise.

Preparation of the Au NDs for Ethanol Oxidation. The GCE was mechanically polished following published procedures.[33] For the preparation of Au NDs, a typical experiment was performed under the deposition potential of 0.0 V for 600 s in 0.5 M H_2SO_4 containing 2.5 mM $HAuCl_4$ and 150 mM EDA. After electrodeposition, the electrodes were washed with water and dried by nitrogen. For comparative study, polycrystalline Au nanoparticles modified GCE were prepared under the same conditions, without EDA.

Furthermore, the electrocatalytic experiments were conducted on the as-prepared Au NDs electrode in 0.5 M NaOH as the electrolyte solution. In order to guarantee the reproducibility, all experiments were preformed for at least three times.

RESULTS AND DISCUSSION

Construction and Characterization of the Au NDs. Figure 1 shows the SEM and TEM images of Au NDs straightforwardly electrodeposited on the GCE from $HAuCl_4$

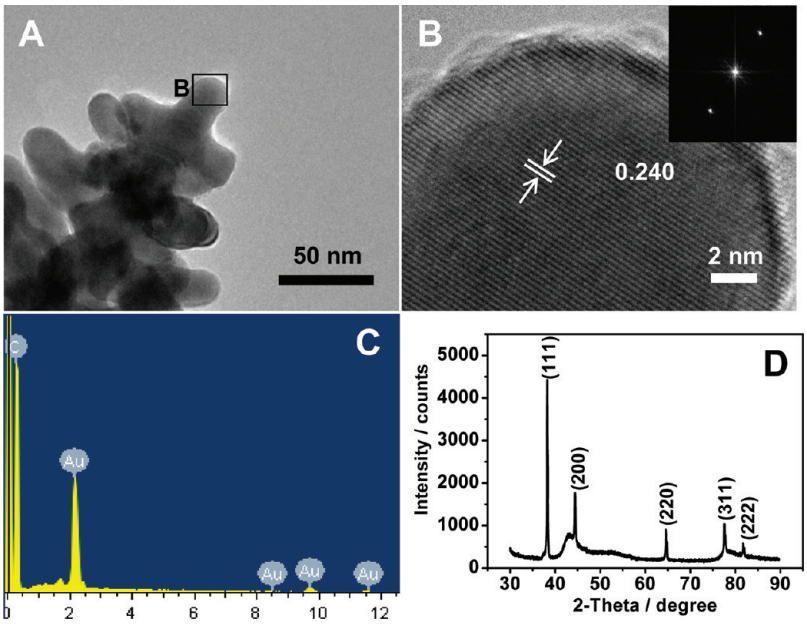

Figure 2. TEM image (A) of an Au sprout; HRTEM image (B) of the tips of the branch marked in (A) (The inset shows the corresponding Fourier transformation pattern of the tip region); EDX spectrum (C); and XRD patterns of the as-synthesized Au NDs obtained under typical conditions (D).

solution containing 0.5 M H_2SO_4 and 150 mM EDA, using the applied potential of 0.0 V (vs SCE), which is more positive than that using cysteine with the applied potential of −0.8 V.[29] Obviously, well-defined dendritic structures are arranged along a backbone with symmetrical side branches. Furthermore, high-magnification SEM images (Figure 1B and D) reveal the detail of the dendrites. Interestingly, there are some "new" branches have grown on the "old" ones.

Meanwhile, to characterize the chemical composition of the Au dendrites, energy dispersive X-ray (EDX) spectrograms were recorded and analyzed. Specifically, element mapping by EDX is used to record the elemental composition of the dendritic surface. The spectrogram of the EDX measurement shows that the characteristic peaks of the metallic Au and carbon (Figure 2C, the carbon present here is ascribed to the GCE). These results demonstrate that the Au dendrites only include Au element, revealing high purity of Au dendrites. Namely, the Au dendrites possess "clean" surfaces.

XRD analysis was performed to characterize chemical composition and crystal structure of the as-prepared Au dendrities (Figure 2D). There are five sharp and strong diffraction peaks observed at 38.2°, 44.4°, 64.6°, 77.6°, and 81.7°, which are assigned to the (111), (200), (220), (311), and (222) planes of the face-centered cubic (fcc) Au (JCPDS 04−0784), respectively. The ratios of the peak intensities due to the (111) planes relative to the (200) and (220) planes are 2.5 and 4.9, respectively. These values are larger than those from Au nanoparticles (1.9 and 3.1, respectively).[29] The XRD results demonstrate that the Au dendrites include pure and well-crystallized gold nanocrystals, and preferentially growing along the (111) planes.

The crystal orientation and growth direction of the Au dendrites were studied by low- and high resolution transmission electron microscopy (HRTEM). Figure 2 shows the thin tip of the main trunk of a single gold dendrite, which enables an examination of its growth direction. As can be seen (Figure 2B), the trunk tip shows clear lattice fringes with the same orientation and spacing. Furthermore, the corresponding Fourier transformation pattern of the tip region is also confirmed this fact. The *d* value of the (111) lattice spacing of the fcc Au crystals is 0.240 nm, consistent with other Au nanostructures in the literature.[29]

In addition, as shown in Figure S1 (Supporting Information), the results from EDS analysis coupled with TEM has also proved that only the characteristic peaks of the metallic gold (2.2. 8.0, 9.7, and 11.4 keV) are detected, revealing the as-formed Au dendrites with high purity, since no peaks come from foreign element.

Figure 3 shows the typical cyclic voltammograms (CVs) recorded in 0.5 M H_2SO_4 solution. The CVs of the Au NDs

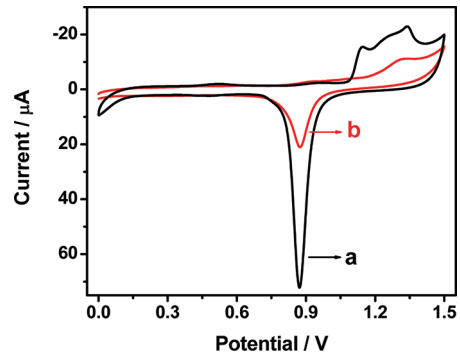

Figure 3. CVs of the Au NDs (curve a) and polycrystalline Au nanoparticles (curve b) modified electrodes in 0.5 M H_2SO_4 with a scan rate of 50 $mV \cdot s^{-1}$.

electrode (curve a) displays the characteristic peaks of Au. There are three oxidation peaks detected at 1.14, 1.24, and 1.34 V, respectively. These peaks are assigned to the oxidation from metallic Au to Au^{3+} ion. The oxidation peak at 1.34 V is quite strong and sharp, while the oxidation peak at 1.24 V is relatively too weak to notice. These observations are different from the

dx.doi.org/10.1021/am3002346 | ACS Appl. Mater. Interfaces 2012, 4, 2570−2576

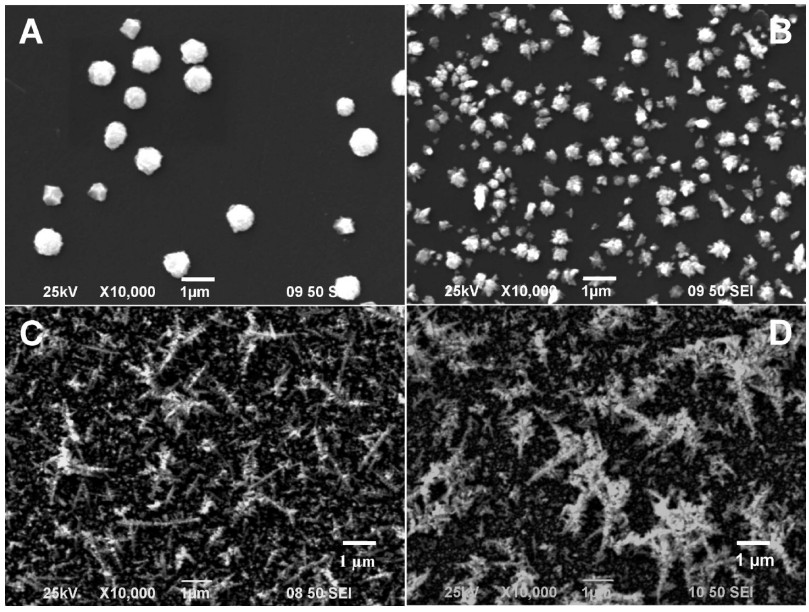

Figure 4. SEM images of the Au deposits obtained at different applied potentials: 0.4 V (A), 0.2 V (B), −0.2 V (C), and −0.6 V (D).

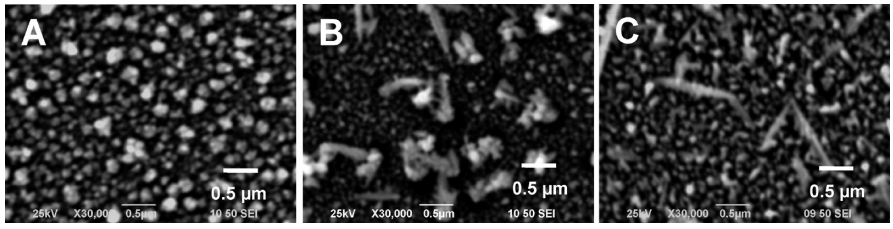

Figure 5. SEM images of the Au deposits prepared with different concentrations of EDA: without (A), with 50 mM (B), and 300 mM (C) EDA.

polycrystalline Au nanoparticles deposited on the GCE (curve b).

Furthermore, the real area of the modified electrode can be estimated from Coulombic integration of the reductive peaks of the gold oxide formed in the positive potentials. The real areas of the Au dendrites and polycrystalline Au nanoparticles modified electrodes were 0.153 and 0.094 cm^2, respectively. As comparison, we also calculated the real area of the bare GCE with a value of 0.062 cm^2, based on the CVs recorded in 1.0 mM $K_3[Fe(CN)_6]$ at different scan rate.[34] Evidently, the Au NDs have larger real area, which is ascribed to the special dendritic nanostructures.

To better understand the growth mechanism of the Au NDs, we have investigated some electrodeposition conditions, such as applied potential, composition of electrolyte and its concentrations, as well as electrodeposition time.

Applied potential is essential to morphology control of the Au deposits. Since initial stage of nucleation and crystal growth behavior of Au are closely associated with the apparent current efficiency. For electrochemical nucleation, two limiting cases of instantaneous and progressive nucleation should be distinguished. For the former, the nuclei number quickly reaches a value that is constant, while in the latter case, new nuclei are continuously formed. Therefore, the final morphology of Au deposit strongly depends on the potential applied on the electrode.[35]

In general, applied potential is optimized based on the reduction peak potential from the CVs. As shown in Figure S2 (Supporting Information), the CVs indicate that applying a potential below 0.82 V would induce the deposition of Au. That is, the reduction of Au^{3+} ion to Au occurs at 0.82 V, and reaches the maximum at 0.65 V. It means that deposition of Au can be feasible upon applying a potential below 0.65 V under suited conditions.

As shown in Figure 4, when the applied potential is 0.4 V, there are some irregular nanoparticles with rough surface and a broad size range from 500 nm to 1 μm (Figure 4A). Using the potential of 0.2 V (Figure 4B), there are multibranched nanoparticles, rather than spherical Au particles. When the potential drops to −0.2 V (Figure 4C), dendritic Au nanostructures are appeared, but smaller than those prepared under typical conditions (Figure 1A). At −0.6 V, the products include many significantly large, rough, and dense Au dendrites (Figure 4D). Meanwhile, there are a large amount of irregular Au nanoparticles observed.

Moreover, the catalytic activity of the Au deposits is closely determined by their sizes and shapes. In our research, the Au nanodendrites prepared at 0.0 V display better catalytic capability toward ethanol oxidation. The catalytic currents are all decreased on the Au deposits prepared by applying lower or higher applied potentials (Figure S3, Supporting Information). Particularly, more negative potential would make more interfering species reduced together on the electrode surface, which affects the quality of the Au deposits. In addition, hydrogen would be likely to generate, which influences the morphology of the Au deposit at more negative potentials.

Furthermore, the effects of EDA and its concentrations are also studied through SEM experiments, while the other

dx.doi.org/10.1021/am3002346 | ACS Appl. Mater. Interfaces 2012, 4, 2570−2576

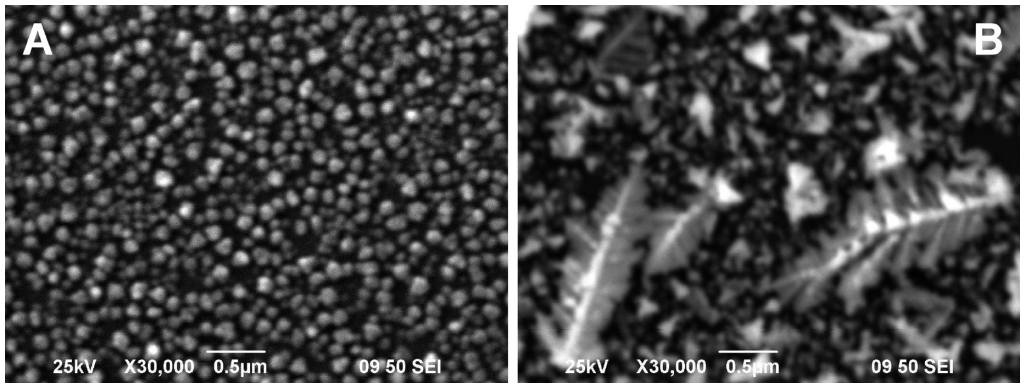

Figure 6. SEM images of the Au NDs prepared with different $HAuCl_4$ concentrations: 0.5 mM $_4$ (A) and 4 mM (B) $HAuCl_4$.

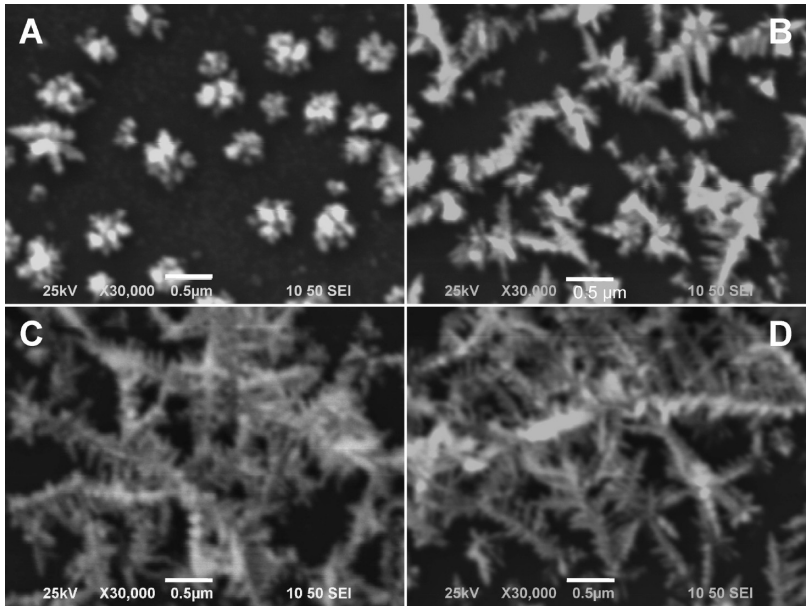

Figure 7. SEM images of the Au NDs for different electrodeposition time: 60 s (A), 180 s (B), 900 s (C), and 1200 s (D).

experimental conditions kept constant (Figure 5). Without EDA, irregular Au nanoparticles are observed (Figure 5A), revealing no preferentially growth along a specific crystallographic direction. The growth rate of Au is isotropic. Using insufficient EDA (below 150 mM), such as 50 mM, a few of tiny dendrites are formed, accompanied by a variety of branched nanoparticles (Figure 5B). Conversely, in the presence of sufficient EDA (e.g., 300 mM), there are sparse and very short dendrites left, as well as many smaller particles (Figure 5C).

A comparative study was conducted by changing the concentrations of $HAuCl_4$, while the other conditions are constant (Figure 6). When the amount of $HAuCl_4$ is below the optimal concentration (2.5 mM), such as 0.5 mM, there are a lot of particles with the diameter of 100−300 nm, while nearly no dendrites are detected (Figure 6A). Alternatively, increasing $HAuCl_4$ concentrations over 4.0 mM (Figure 6B), a large number of seed-like Au nanocrystals are formed, accompanied with a couple of dendrites. These SEM experiments (Figures 5 and 6) confirm that only proper ratios of EDA with $HAuCl_4$ in a certain concentration range are desired in the synthesis of Au dendrites.

Figure 7 shows the morphological evolution of the dendritic nanostructures with deposition time. With time increasing, there is a tendency that the Au nanostructures grow more and more complex (Figure 7A−D). After 60 s, many multibranched crystals of ∼400 nm in size are appeared, which are built with several smaller particles (Figure 7A). When the deposition continues for 180 s, some short dendrites are detected (Figure 7B). It indicates that further growth occurs from the original multibranched crystals. Clearly, the dendritic structures stay at the evolutional stage of growth. When the deposition time is prolonged to 1200 s, the obtained dendrites become very big and irregular (Figure 7D). Therefore, 600 s was chosen as the optimal deposition time.

Taken all the above results together, we find that morphology control at the crystallographic level can be achieved by fine-adjusting the reaction conditions (including applied potential, composition of electrolyte and its concentrations, and electrodeposition time). In our research, the growth of Au dendrites with EDA is explained by a two-staged growth model: initial branching and subsequent dendritic growth. At first stage, many Au nuclei are randomly grown on the electrode surface via instantaneous reduction of $AuCl_4^-$ ion to metallic Au. The adjacent EDA molecule is quickly formed a monolayer on the surface of Au nuclei by self-assembly, and prevented aggregation. The self-assembled monolayer causes nonequilibrium system and thereby prefers the formation of

dx.doi.org/10.1021/am3002346 | ACS Appl. Mater. Interfaces 2012, 4, 2570−2576

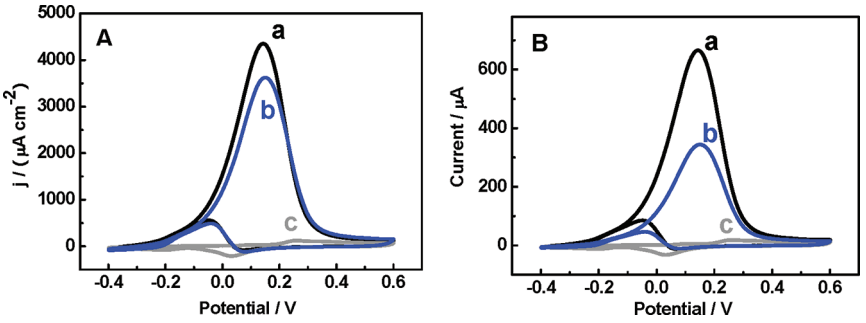

Figure 8. (A) CVs of the Au NDs (curve a, c) and polycrystalline Au nanoparticles (curve b) modified electrodes in the presence (curve a, b) and absence (curve c) of 1.0 M ethanol. (B) The CVs of the Au NDs (curve a, c) and polycrystalline Au nanoparticles (curve b) modified electrodes with (curve a, b) and without (curve c) 1.0 M ethanol. Scan rate: 50 mV·s^{-1}. Electrolyte: 0.5 M NaOH.

dendrites. Moreover, two $-NH_2$ groups in EDA molecule and adjacent together are likely to form branched nanostructures, which enlarge the branching power of EDA.[36] Thus, EDA molecule acts as a shape-directing agent for initial branching. Then, the dendritic growth occurs at the initial tips and trunks of the branched structures, which is predominated by kinetically controlling. To our knowledge, nucleation, adsorption, and branching are fast processes, and hence the morphology adjustment is the later stage of a slow process dominated by the kinetic model. Evidently, the growth mechanism of the Au NDs is quite distinguished from that using cysteine.[29] Since cysteine molecule has strong adsorption on the (100) and (110) facets, and thereby the electrodeposition of Au is seriously inhibited on these planes. Whereas, the (110) planes of Au is free of cysteine, resulting into the growth of the Au nanocrystals preferentially along the (111) directions.

Electrocatalytic Activity of the Au NDs. It is known that gold nanomaterials have catalytic activity toward oxygen reducing.[11,22,24,28,37] Recently, people find that Au nanocrystals also exhibit good catalytic performance toward methanol or ethanol oxidation, which strongly depend on their size and morphology.[10,38−40]

The electrocatalytic behavior of the Au NDs electrodes was investigated in 0.5 M NaOH solution containing 1.0 M ethanol and compared with the catalytic activity of the polycrystalline Au nanoparticles modified electrode prepared under the identical conditions in the absence of EDA (Figure 8). A broad oxidation peak is observed at 0.26 V and a reduction peak appears at 0.03 V (Figure 8, curve c), corresponding to the oxidation and reduction of gold, respectively.[30] The Au NDs electrode performs much better electrocatalytic ability and the onset potential of ethanol oxidation at 0.14 V (Figure 8, curve a), negative shift in comparison with the polycrystalline Au nanoparticles modified electrode with a value of 0.15 V (Figure 8, curve b) because of the dendritic hierarchical nanostructures. Besides, the current density of the Au dendrites (curve a, Figure 8A) is higher than the polycrystalline Au nanoparticles, revealing larger surface area of the Au dendrites (curve b, Figure 8A). Similarly, the catalytic currents of the Au dendrites (curve a, Figure 8B) are higher than the polycrystalline Au nanoparticles (curve b, Figure 8B). Furthermore, the onset potential of ethanol oxidation is also more negative, compared to that of the dendritic gold microstrutures electrodeposited on an indium tin oxide substrate with a value of 0.38 V.[30] These results reveal high activity of the Au NDs in our system.

In general, smaller ratio of the peak current density (j_f) in the forward potential scan and the peak current density (j_r) in the reverse scan (that is, j_r/j_f), would bring better poisoning-resistance of the electrodes for ethanol oxidation. The oxidation peak in the backward scan corresponds to the electrochemical oxidation of CO and other adsorbed species.[41,42] The value for j_r/j_f on the Au NDs electrode is 0.12 (Figure 8B), which is smaller than that on the polycrystalline Au nanoparticles modified electrode (0.14). Moreover, this value is much smaller than the Au microdendrites electrodeposited on indium tin oxide substrates (0.27) and bare gold electrode (0.64),[30] showing that the Au NDs electrode has better poisoning-resistance and steady-state behavior for ethanol oxidation.

Figure 9 shows the typical CVs obtained at the Au NDs electrode with successive addition of ethanol into the blank 0.5

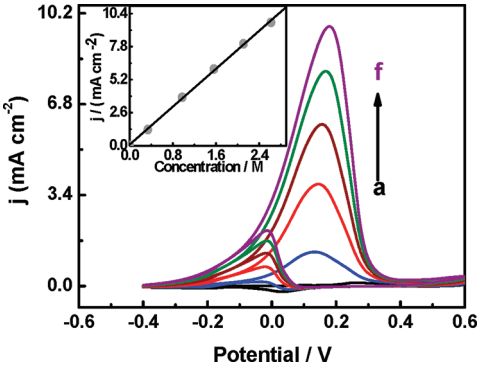

Figure 9. Catalytic responses of the Au NDs electrode without (curve a) and with different concentrations of ethanol: 0.33 M (curve b), 1.0 M (curve c), 1.6 M (curve d), 2.1 M (curve e), and 2.6 M (curve f) in 0.5 M NaOH. Scan rate: 50 mV·s^{-1}. Inset: The relationship of the catalytic current density with ethanol concentration.

M NaOH solution. After injection of ethanol into the solution, the Au NDs electrode responds quickly (less than 0.1 s) to reach 95% of the maximum current. At the same time, the corresponding catalytic currents increase linearly up to the ethanol concentrations of 6.2 M. The calibration curve was obtained via three times of parallel measurements (Inset in Figure 9). The resulting slope (sensitivity) and correlation coefficient are 8.08 mA·M^{-1}·cm^{-2} and 0.9995, respectively. In addition, for three Au NDs electrodes prepared independently, the catalytic currents are similar under the same conditions, indicating good reproducibility.

Additionally, the effects of EDA on the catalytic oxidation of ethanol were tested by applying a potential of −1.2 V to remove the possible adsorbed EDA. It is interesting to find that nearly no different can be found before and after this treatment. This is due to weak interactions of Au dendrites with $-NH_2$

groups in EDA molecule, compared to the S−Au bond when using cysteine in the literature.[29] In their system, cysteine molecule has to be removed by applying a potential of −1.2 V. Thus, the as-prepared Au dendrites in our work possess "clean" surfaces, and thereby can be directly used for catalysis measurements, free of any special pretreatment.

As well-known, the interactions between EDA and Au NDs EDA are very weak, compared to the S−Au bond in the literature.[29] As expected, our catalytic experiments also demonstrate this assumption (Figure S4, Supporting Information). The effects of EDA on the catalytic oxidation of ethanol were tested by applying a potential of −1.2 V to remove the possible adsorbed EDA. It is interesting to find that nearly no different can be found before and after this treatment. However, in their system, the catalytic ability greatly improved after removing the adsorbed cysteine using a very negative potential of −1.2 V.[29] Therefore, the Au NDs possess "clean" surfaces, and thereby can be directly used for catalytic measurements, without any special pretreatment.

CONCLUSION

In the presence of EDA, Au NDs were prepared via low-potential synthesis, without using any organic solvent or surfactant. The size, shape, and crystal orientation of the Au deposits are essentially related with the electrolyte and its concentrations, as well as applied potential and electrodeposition time. A two-staged growth mechanism of initial branching and dendritic growth was proposed. The "clean" surface of the as-synthesized Au NDs endows them excellent catalytic ability toward ethanol oxidation. Additionally, the dendritic Au structures provide a promising platform to design and construct multifunctional devices for potential applications in catalysis, SERS, and biomedical images.

ASSOCIATED CONTENT

Supporting Information

Typical EDS spectrum of the as-synthesized Au NDs, cyclic voltammograms of a GCE in a solution of 2.5 mM $HAuCl_4$ and 0.5 M H_2SO_4, and a polycrystalline Au electrode in a solution ontaining 150 mM EDA are available as Supporting Information. This information is available free of charge via the Internet at http://pubs.acs.org/.

AUTHOR INFORMATION

Corresponding Author

*E-mail: ajwangnju@gmail.com.

Notes

The authors declare no competing financial interest.

ACKNOWLEDGMENTS

This work was financially supported by the NSFC (Nos. 20805011, 20905021, 21175118), the Foundation of the Ministry of Education of China for Returned Scholars (A.J.W. and J.J.F.), and the opening funding of State Key Laboratory of Analytical Chemistry for Life Science of Nanjing University (SKLACLS1107 for J.J.F.).

REFERENCES

(1) Feng, J. J.; Gernert, U.; Hildebrandt, P.; Weidinger, I. M. *Adv. Funct. Mater.* **2010**, *20*, 1954−1961.
(2) Zhao, J.; Zhang, X.; Yonzon, C. R.; Haes, A. J.; Van Duyne, R. P. *Nanomedicine* **2006**, *1*, 219−228.
(3) Yun, S.; Oh, M. K.; Kim, S. K.; Park, S. *J. Phys. Chem. C* **2009**, *113*, 13551−13557.
(4) Yoon, I.; Kang, T.; Choi, W.; Kim, J.; Yoo, Y.; Joo, S.-W.; Park, Q. H.; Ihee, H.; Kim, B. *J. Am. Chem. Soc.* **2008**, *131*, 758−762.
(5) Wang, C. H.; Song, Y. Y.; Zhao, J. W.; Xia, X. H. *Surf. Sci.* **2006**, *600*, 38−42.
(6) Chen, M.; Wu, B.; Yang, J.; Zheng, N. *Adv. Mater.* **2012**, *24*, 862−879.
(7) Raj, C. R.; Jena, B. K. *Chem. Commun.* **2005**, 2005−2007.
(8) Jena, B. K.; Raj, C. R. *Chem.—Eur. J.* **2006**, *12*, 2702−2708.
(9) Sau, T. K.; Rogach, A. L. *Adv. Mater.* **2010**, *22*, 1781−1804.
(10) Jena, B. K.; Raj, C. R. *Langmuir* **2007**, *23*, 4064−4070.
(11) Daniel, M. C.; Astruc, D. *Chem. Rev.* **2003**, *104*, 293−346.
(12) Yoo, S. M.; Kang, T.; Kang, H.; Lee, H.; Kang, M.; Lee, S. Y.; Kim, B. *Small* **2008**, *7*, 3254−3254.
(13) Huang, Z.; Meng, G.; Huang, Q.; Yang, Y.; Zhu, C.; Tang, C. *Adv. Mater.* **2010**, *22*, 4136−4139.
(14) Lu, G.; Li, C.; Shi, G. *Chem. Mater.* **2007**, *19*, 3433−3440.
(15) Hu, Y.; Pan, N.; Zhang, K.; Wang, Z.; Hu, H.; Wang, X. *Phys. Status Solidi A* **2007**, *204*, 3398−3404.
(16) Qin, Y.; Song, Y.; Sun, N.; Zhao, N.; Li, M.; Qi, L. *Chem. Mater.* **2008**, *20*, 3965−3972.
(17) Tang, X. L.; Jiang, P.; Ge, G. L.; Tsuji, M.; Xie, S. S.; Guo, Y. J. *Langmuir* **2008**, *24*, 1763−1768.
(18) Zhang, J.; Meng, L.; Zhao, D.; Fei, Z.; Lu, Q.; Dyson, P. J. *Langmuir* **2008**, *24*, 2699−2704.
(19) Pan, M.; Sun, H.; Lim, J. W.; Bakaul, S. R.; Zeng, Y.; Xing, S.; Wu, T.; Yan, Q.; Chen, H. *Chem. Commun.* **2012**.
(20) Guo, S.; Wang, E. *Nano Today* **2011**, *6*, 240−264.
(21) Ye, J.; Hutchison, J. A.; Uji-i, H.; Hofkens, J.; Lagae, L.; Mazes, G.; Borghs, G.; Van Dorpe, P. *Nanoscale* **2012**.
(22) Huang, D.; Bai, X.; Zheng, L. *J. Phys. Chem. C* **2011**, *115*, 14641−14647.
(23) Huang, T.; Meng, F.; Qi, L. *Langmuir* **2009**, *26*, 7582−7589.
(24) Bai, X.; Gao, Y.; Liu, H.-g.; Zheng, L. *J. Phys. Chem. C* **2009**, *113*, 17730−17736.
(25) Xu, X.; Jia, J.; Yang, X.; Dong, S. *Langmuir* **2010**, *26*, 7627−7631.
(26) Sheffer, M.; Mandler, D. *Electrochim. Acta* **2009**, *54*, 2951−2956.
(27) Li, F.; Han, X.; Liu, S. *Biosens. Bioelectron.* **2011**, *26*, 2619−2625.
(28) Guo, S.; Wang, E. *Anal. Chim. Acta* **2007**, *598*, 181−192.
(29) Lin, T. H.; Lin, C. W.; Liu, H. H.; Sheu, J. T.; Hung, W. H. *Chem. Commun.* **2011**, *47*, 2044−2046.
(30) Ye, W.; Yan, J.; Ye, Q.; Zhou, F. *J. Phys. Chem. C* **2010**, *114*, 15617−15624.
(31) Huan, T. N.; Ganesh, T.; Kim, K. S.; Kim, S.; Han, S.-H.; Chung, H. *Biosens. Bioelectron.* **2011**, *27*, 183−186.
(32) Chen, X.; Wang, Y.; Zhou, J.; Yan, W.; Li, X.; Zhu, J.-J. *Anal. Chem.* **2008**, *80*, 2133−2140.
(33) Feng, J. J.; Xu, J. J.; Chen, H. Y. *Biosens. Bioelectron.* **2007**, *22*, 1618−1624.
(34) Ju, H.; Liu, S.; Ge, B.; Lisdat, F.; Scheller, F. W. *Electroanal.* **2002**, *14*, 141−147.
(35) Depestel, L. M.; Strubbe, K. *J. Electroanal. Chem.* **2004**, *572*, 195−201.
(36) Xiao, J.; Qi, L. *Nanoscale* **2011**, *3*, 1383−1396.
(37) Polshettiwar, V.; Baruwati, B.; Varma, R. S. *ACS Nano* **2009**, *3*, 728−736.
(38) Maye, M. M.; Luo, J.; Lin, Y.; Engelhard, M. H.; Hepel, M.; Zhong, C.-J. *Langmuir* **2002**, *19*, 125−131.
(39) Narayanan, R.; El-Sayed, M. A. *J. Phys. Chem. B* **2005**, *109*, 12663−12676.
(40) Zhang, J.; Liu, P.; Ma, H.; Ding, Y. *J. Phys. Chem. C* **2007**, *111*, 10382−10388.
(41) Leung, L. W. H.; Weaver, M. J. *J. Phys. Chem.* **1988**, *92*, 4019−4022.
(42) Iwasita, T. *Electrochim. Acta* **2002**, *47*, 3663−3674.